Journal of Crystal Growth 419 (2015) 37–41

Contents lists available at ScienceDirect

Journal of Crystal Growth

journal homepage: www.elsevier.com/locate/jcrysgro

Single crystal growth and characterization of $GdRh_2Si_2$

K. Kliemt*, C. Krellner

Kristall- und Materiallabor, Physikalisches Institut, Goethe-Universität Frankfurt, Max-von-Laue Stasse 1, 60438 Frankfurt am Main, Germany

ARTICLE INFO

Article history:
Received 24 December 2014
Received in revised form
15 February 2015
Accepted 22 February 2015
Communicated by Pierre Müller
Available online 5 March 2015

Keywords:
A2. Bridgman technique
A2. Growth from high-temperature solutions
A2. Single crystal growth
B1. Gadolinium compounds
B2. Magnetic materials
B1. Rare earth compounds

ABSTRACT

High-temperature indium flux growth was applied to prepare single crystals of $GdRh_2Si_2$ by a modified Bridgman method leading to mm-sized single crystals with a platelet habitus. Specific heat and susceptibility data of $GdRh_2Si_2$ exhibit a pronounced anomaly at $T_N = 107$ K, where the antiferromagnetic ordering sets in. Magnetic measurements on the single crystals were performed down to $T=2$ K in external fields from $B=0$ to 9 T applied along the [100]-, [110]- and [001]-direction of the tetragonal lattice. The effective magnetic moment determined from a Curie–Weiss fit agrees well with experimental values from literature, but is larger than the theoretically predicted value. Electrical transport data recorded for current flow parallel and perpendicular to the [001]-direction show a large anisotropy below T_N. The residual resistivity ratio $RRR = \rho_{300\,K}/\rho_0 \sim 23$ demonstrates that we succeeded in preparing high-quality crystals using high-temperature indium flux-growth.

1. Introduction

Among the ternary silicides of the type RT_2Si_2 (R=rare earth, T=transition metal) which crystallize in the body-centered tetragonal $ThCr_2Si_2$ structure, $GdRh_2Si_2$ has attracted much attention in the last decades as it belongs to the compounds with rare earth elements with exceptional magnetic properties, e.g., $CeRh_2Si_2$ [1], $YbRh_2Si_2$ [2] and $EuRh_2Si_2$ [3,4]. Studies of Gd-compounds are of special interest since the 4*f* shell of Gd is half filled and therefore its ground state with $S=7/2$ and $L=0$ is insensitive to crystal-electric-field (CEF) effects. In the past, polycrystalline $GdRh_2Si_2$ was subject to several investigations. Magnetization and Mössbauer studies were performed by Felner and Nowik [5,6] examining the series RRh_2Si_2 and by Czjzek et al. [7] with focus on the properties of the transition metal T in the compounds GdT_2Si_2. From Mössbauer spectra of ^{155}Gd in $GdRh_2Si_2$ it was deduced that the rare earth local moments order antiferromagnetically with the ordering in the basal plane perpendicular to the four-fold symmetry axis of the tetragonal lattice [5,6]. It is known from neutron diffraction experiments that the antiferromagnetic (AFM) properties in the series RRh_2Si_2 arise due to a stacking of ferromagnetic layers [8]. Pressure studies by Szytuła et al. [9] revealed that the Néel temperature of $GdRh_2Si_2$ decreases with increasing applied pressure. An ESR-study was performed by Kwapulinska et al. [10] and they found that the *g*-factor is temperature independent from T_N to 300 K with $g = 1.995 \pm 0.01$. Recently, the magnetic properties of $GdRh_2Si_2$ were investigated by hyperfine interactions and magnetization measurements [11].

All measurements up to now were carried out on polycrystalline material since single crystals were not available. Here, we report on the successful crystal growth and present a detailed study of the magnetic and electrical transport properties of $GdRh_2Si_2$ single crystals. The crystals were grown using a high-temperature indium-flux technique [13,12]. The crystal growth set up was chosen similar to that applied for the single crystal growth of $YbRh_2Si_2$ [14].

2. Experimental details

Single crystals of $GdRh_2Si_2$ were grown in In flux. The high purity starting materials Gd (99.9%, Johnson Matthey), Rh (99.9%, Heraeus), Si (99.9999%, Wacker), with the molar ratio of 1:2:2, and In (99.9995%, Schuckard) were weighed in a graphite crucible and sealed in a tantalum crucible under argon atmosphere (99.999%). The stoichiometric composition of the elements was used with 96 at% indium as flux. The experimental setup of the crucible (with a volume of 10 ml) is shown in the left inset of Fig. 1. Indium was put on the bottom of the crucible covered by the high-melting elements Rh and Si covered again by In pieces. Subsequently, the crucible was transferred to the Ar-filled glove-box, where Gd was placed on top, covered once more by In. Finally, the Ta-crucible

* Corresponding author. Tel.: +49 69 798 47255.
E-mail address: kliemt@physik.uni-frankfurt.de (K. Kliemt).

http://dx.doi.org/10.1016/j.jcrysgro.2015.02.079
0022-0248/

was closed using arc-welding. The filled Ta-crucible was put under a stream of Ar in a resistive furnace (GERO HTRV 70–250/18) and the elements were heated up to 1550 °C. The melt was homogenized for 1 h and then cooled by slow moving of the whole furnace with 1 mm/h leading to a cooling rate in the range of 0.5–4 K/h down to 1000 °C, while the position of the crucible stayed fixed. During the growth, the temperature was measured at the bottom of the tantalum crucible by a thermocouple of type B. In Fig. 1 the recorded temperature–time profile is depicted. The crucible holder made from Al_2O_3 together with the tip of the thermocouple in the center is shown in the right inset. After the growth, the excess flux was removed with diluted HCl. The crystal structure was characterized by powder X-ray diffraction on crushed single crystals, using $Cu-K_\alpha$ radiation. The chemical composition was checked by energy-dispersive X-ray spectroscopy (EDX). The orientation of the single crystals was determined using a Laue camera with X-ray radiation from a tungsten anode. Four-point resistivity, magnetization, and heat-capacity measurements were performed using the commercial measurement options of a Quantum Design PPMS.

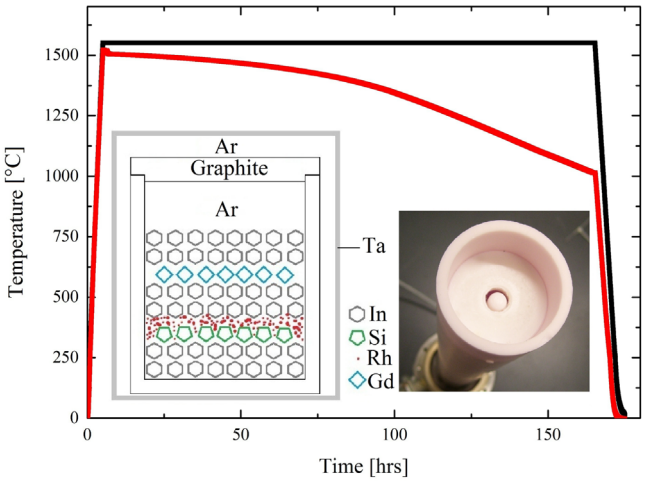

Fig. 1. Measured temperature–time-profiles for a growth experiment (red curve) and furnace temperature (black curve). Inset on the right: Picture of the platform on which the crucible is mounted during the growth. The temperature was measured with a thermocouple directly at the bottom of the crucible. Inset on the left: Schematic arrangement of the elements in the crucible system for the crystal growth of $GdRh_2Si_2$. The inner crucible is made from graphite, enclosed under argon in a Ta-crucible. (For interpretation of the references to color in this figure caption, the reader is referred to the web version of this paper.)

3. Results and discussion

3.1. Crystal growth

Until now, the successful single crystal growth was not reported, which probably is due to the incongruent melting of this material at temperatures above 2000 °C. We therefore employed the flux-growth technique, which allows us to perform the crystal growth at temperatures below the high melting points of the elements (Gd 1312 °C, Rh 1964 °C, and Si 1414 °C). No information was found in the literature about the melting point of $GdRh_2Si_2$. So far, it was not possible to determine the accurate crystallization temperature of $GdRh_2Si_2$ in 96 at% In, but a systematic optimization of the starting temperature revealed that the largest crystals could be grown when starting the crystal growth at $T_{start} = 1520$ °C, compared to growths starting below 1500 °C. The optimized temperature–time profile is depicted in Fig. 1.

After cooling, the excess In is dissolved by hydrochloric acid until phase pure $GdRh_2Si_2$ is obtained. Although, not everything of the starting material was crystallized in the $GdRh_2Si_2$ phase, the resulting single crystals of $GdRh_2Si_2$ are already large enough to carry out several physical characterization measurements as described above. A typical single crystal has a platelet habitus with the shortest dimension, 200–500 µm, along the crystallographic *c*-direction, as shown in Fig. 2a. For larger crystals a more thorough optimization of the crystal growth needs to be undertaken. In Ref. [14] it was described how this problem was investigated for the related compound $YbRh_2Si_2$. There, it was found that better results were obtained by changing the initial Rh: Si ratio of the melt.

3.2. Structural and chemical characterization

The single crystals were analyzed with electron microscopy and the secondary electron image indicates the absence of any inclusions of secondary phases (Fig. 2b). From that picture, the formation of

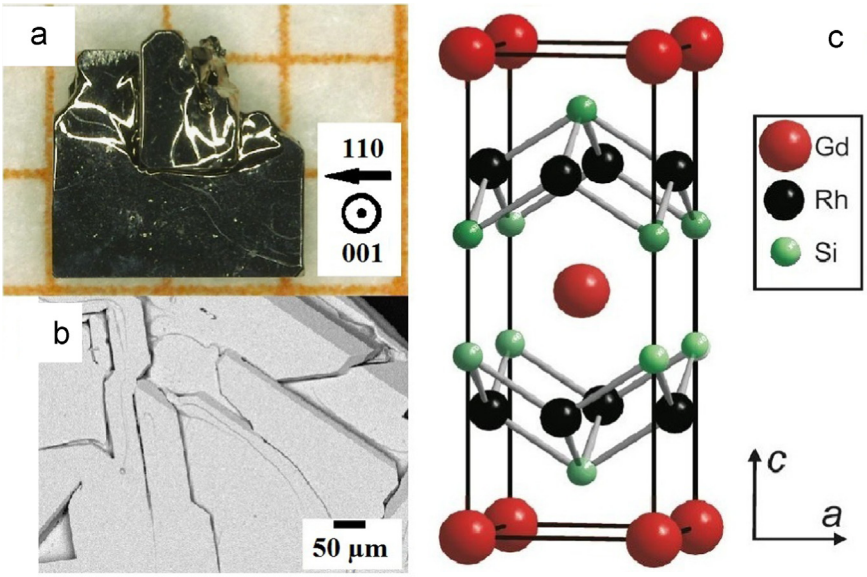

Fig. 2. (a) Optical microscope image of a $GdRh_2Si_2$ single crystal. The largest crystal edges always belong either to the [100]- or the [110]-direction. (b) Electron microscopy (secondary electrons) indicates the phase purity of the crystal. (c) Tetragonal crystal structure of $GdRh_2Si_2$.

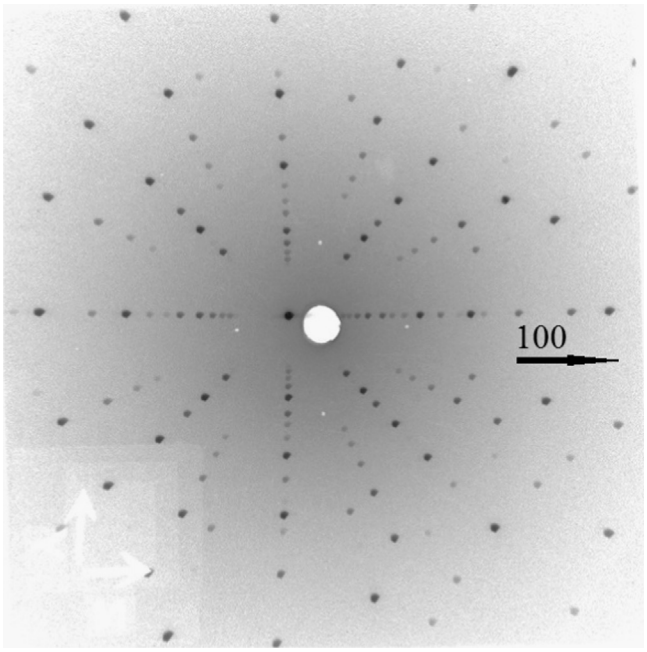

Fig. 3. The Laue pattern of the 001-direction shows the four-fold symmetry. The sharp reflexes are an indicator for the good sample quality.

terraces along the *c*-direction is apparent. The chemical composition determined by EDX microprobe analysis revealed (20 ± 1) at% Gd, (40 ± 1) at% Rh and (40 ± 2) at% Si. We cannot exclude some Rh–Si site exchange within these error bars; however, for the related compound $YbRh_2Si_2$ a detailed structural and chemical analysis was conducted by highly accurate X-ray diffraction and wavelength dispersive X-ray spectroscopy measurements [15]. There, it turned out that the structure accepts some Rh–Si site exchange, with a rather small homogeneity range for Rh, which was found to be 40.0–40.2 at%.

Powder X-ray diffraction measurements confirmed the *I*4/*mmm* tetragonal structure (Fig. 2c) with lattice parameters $a=4.042(2)$ Å and $c=9.986(4)$ Å, which are in agreement with the data published for polycrystalline samples [5,9,11].

The high quality of the single crystals is evident also from a Laue back scattering image, presented in Fig. 3. The central point can be indexed as the (0 0 1) reflex, proving that the direction perpendicular to the surface of the platelets corresponds to the *c*-direction. The sharp points verify that the terraces seen in Fig. 2b do not lead to a slight misalignment along *c*.

3.3. Specific-heat measurements

In Fig. 4 specific-heat data are shown for the two related materials $GdRh_2Si_2$ and $LuRh_2Si_2$. The latter serves as a non-magnetic reference system with a completely filled 4*f*-shell and the data are taken from Ref. [16]. For $GdRh_2Si_2$ a pronounced and sharp λ-type anomaly is observed at T_N, establishing a second order phase transition into the AFM ordered phase. For $T<5$ K the specific heat of $GdRh_2Si_2$ can be well described by $C/T=\gamma_0+\beta T^2$ (cf. inset of Fig. 4) with the Sommerfeld coefficient $\gamma_0\approx4$ mJ/mol K^2 determined from a linear fit to the data. The Debye temperature $\Theta_D\approx148$ K was calculated from the slope β according to $\beta=12\pi^4R/(5\Theta_D^3)$.

3.4. Magnetic measurements

In Fig. 5 susceptibility data as a function of temperature is presented for one single crystal with the magnetic field along the [100]-direction. At small fields ($B\leq0.1$ T) a sharp anomaly is evident

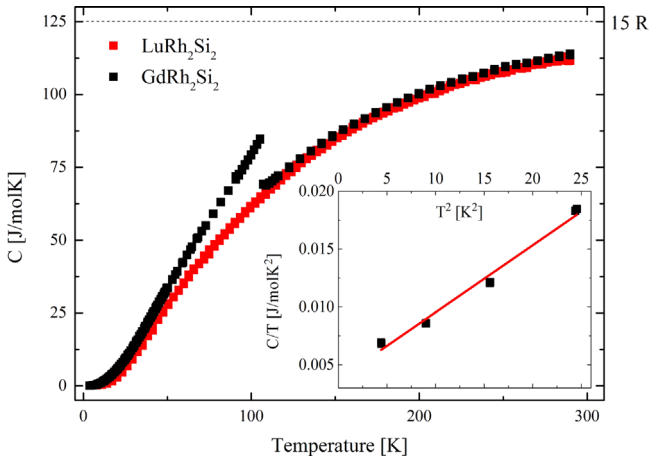

Fig. 4. Specific-heat data as function of temperature for a single crystal of $GdRh_2Si_2$ and polycrystalline $LuRh_2Si_2$ (from Ref. [16]). The inset enlarges the low-temperature part of the specific heat of $GdRh_2Si_2$, plotted as C/T versus T^2. From a linear fit, the Sommerfeld coefficient and the Debye temperature could be extracted.

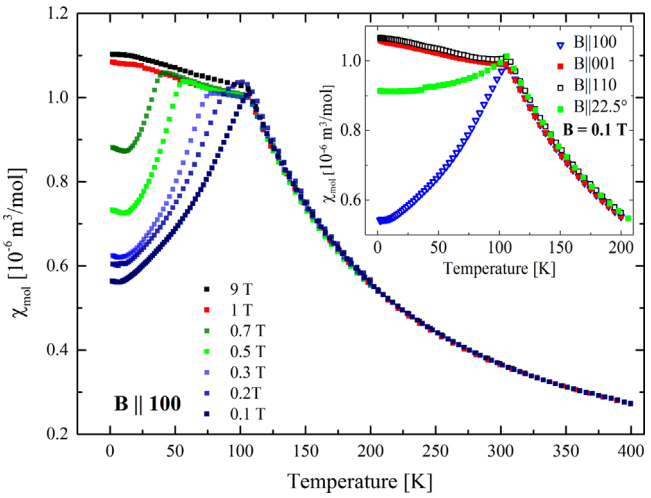

Fig. 5. Susceptibility as a function of temperature for $B\|100$. The spin flop transition shifts towards lower temperatures for higher fields. Inset: Comparison of susceptibility data for an applied field of 0.1 T for 4 different crystal orientations. (For interpretation of the references to color in this figure caption, the reader is referred to the web version of this paper.)

at $T_N=107$ K followed by a strong decrease towards lower temperatures. At higher magnetic fields, $0.1\text{ T}<B<1\text{ T}$, a field-induced anomaly emerges below T_N shifting to lower temperatures with increasing field, visible, e.g., as a pronounced drop at $T^*=50$ K for $B=0.5$ T. Above 1 T, the susceptibility is nearly field independent, and slightly increases with decreasing temperature. This behavior is different for different field directions, as shown in the inset of Fig. 5. Here, $\chi(T)$ is shown for $B=0.1$ T with $B\|100$ (blue open triangles), $B\|110$ (black open squares), $B\|001$ (red closed squares), and B aligned in an angle of 22.5° to the [100]- and the [110]-direction as well as perpendicular to the [001]-direction (green closed squares). Remarkably for $B\|001$ and $B\|110$, $\chi(T)$ is changing only slightly below T_N in contrast to the strong decrease discussed for $B\|100$. The field direction between the [100]- and the [110]-direction was measured to prove that no other in-plane direction shows a more pronounced drop at T_N. A molecular-field analysis of the magnetization for a layered antiferromagnet presented in [17] suggests the alignment of the magnetic moments in $GdRh_2Si_2$ to be along the [100]-direction. This model was not derived for a tetragonal system, therefore, to confirm this scenario, neutron diffraction should be performed on the single crystals. A similar behavior of

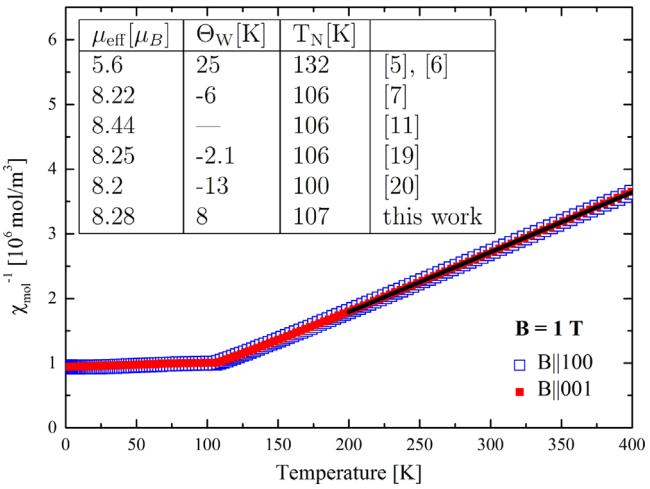

Fig. 6. The figure shows the fit of the inverse susceptibility (black solid line) from which the effective magnetic moment and the Weiss temperature were determined.

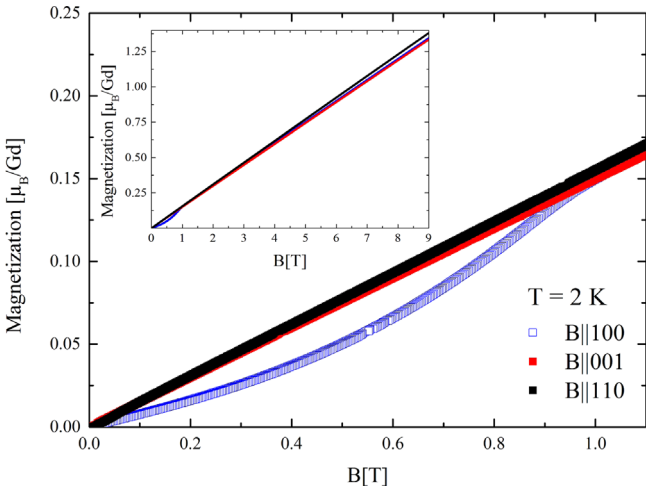

Fig. 7. $M(B)$ data for field applied in 3 different crystal orientations at $T=2$ K. Spin flop in [100]-direction.

the magnetization was reported for the tetragonal compound $EuGa_4$ [18] where the magnetic moments are ordered along the [100]-direction. The authors in [18] assign the occurrence of the metamagnetic transition to the field-induced change of antiferromagnetic domains.

Above 150 K, the susceptibility follows a Curie–Weiss behavior for all measured crystal orientations. The effective magnetic moment, $\mu_{eff} = (8.28 \pm 0.10)\mu_B$, agrees well with published values determined on polycrystalline samples [7,19], and is larger than expected for sole Gd^{3+} ions ($7.94\mu_B$). Furthermore, no anisotropy of the inverse susceptibility above T_N could be resolved in our measurements on single crystals.

The Weiss temperature, Θ_W, was determined from a linear fit of the inverse susceptibility χ^{-1} from 200 to 400 K, shown as solid black line in Fig. 6, which is positive indicating dominantly ferromagnetic exchange interactions, with $\Theta_W = (8 \pm 5)$ K. This is in contrast to the findings of [7,19,20] who reported negative Weiss temperatures. In the inset of Fig. 6 these reported values of the effective magnetic moment μ_{eff} and the Weiss temperature Θ_W are summarized together with our findings.

It is known from earlier work on RRh_2Si_2 compounds [8] that antiferromagnetic properties in this family arise due to a stacking of ferromagnetic layers. From a Mössbauer experiment was deduced that the magnetic moments in $GdRh_2Si_2$ are aligned in the basal plane of the tetragonal structure [6]. In our measurements we found, that there is a sizeable in-plane anisotropy in $M(T)$ and $M(B)$, Figs. 5 and 7. In Fig. 7, $M(B)$ measured for different field directions at $T=2$ K on a $GdRh_2Si_2$ single crystal is shown. For the field applied parallel to the [100]-direction a small spin flop transition can be observed at $B_{sf} \approx 1$ T.

In previous work, some of the compounds RRh_2Si_2 were examined by Felner and Nowik [5,6]. They deduced from magnetization and Mössbauer studies that these compounds have two magnetic phase transitions: one corresponding to the ordering of the rare earth ion and the other one to the itinerant electron ordering of the Rh sublattice. A peak in the susceptibility at about 16 K besides the transition into the AFM ordered state was reported.

The compounds GdT_2Si_2 (T=transition metal) were studied by Czjzek et al. [7] by means of Mössbauer spectroscopy and magnetization measurements. In contrast to Felner and Nowik [5,6], these authors reported that the transition metal ions, with the exception of manganese, do not carry magnetic moments in any of these compounds. They found an enhanced effective magnetic moment of the Gd^{3+}-ions, and proposed the magnetic

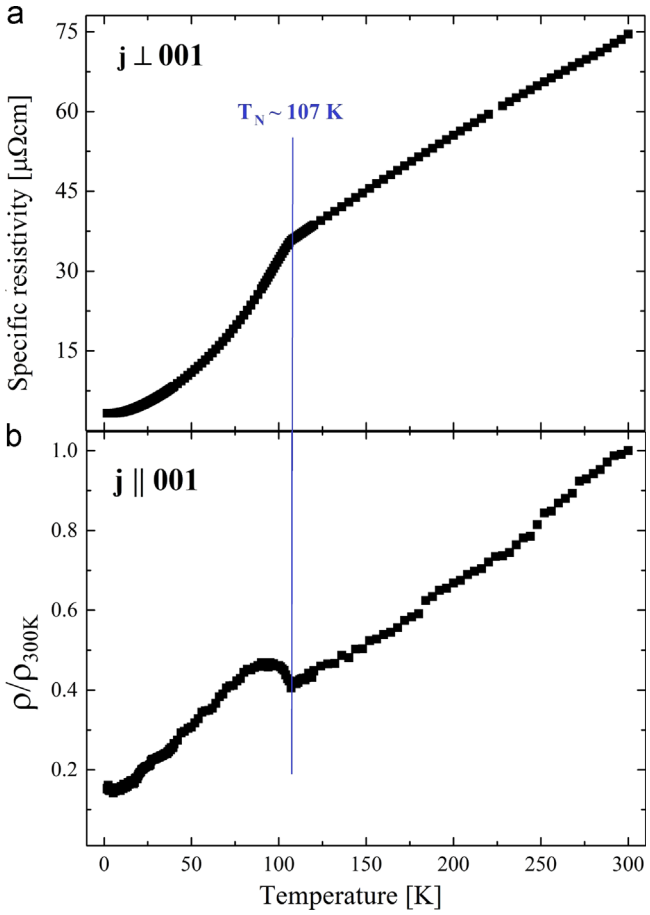

Fig. 8. Electrical resistivity measured for current flow (a) perpendicular and (b) parallel to the [001]-direction. A clear anomaly is visible at T_N which is rather anisotropic for the two current directions.

moments of rare-earth 5*d* electrons induced by 4*f*–5*d* exchange interaction, to be the origin of this additional contribution to the effective moment. XMCD-measurements are presently on the way to answer the question, if the enhancement of the magnetic moment, determined for the Gd^{3+}-ions in $GdRh_2Si_2$, results from a contribution of Gd 5*d* electrons.

Furthermore, a hint to the existence of a second magnetic transition at $T_{II} = 17$ K was reported in Ref. [7]. This statement of

Refs. [5–7] was based on the observation of a cusp in the susceptibility, similar to what we observe for $B \parallel 100$ at about 0.7 T. We have demonstrated that this additional cusp is a field-induced transition, due to the spin flop transition at B_{sf}, which of course is present in a polycrystalline sample as well, if the magnetic field is in a similar range.

3.5. Electrical-transport measurement

$GdRh_2Si_2$ is a tetragonal antiferromagnet with a layered crystal structure (cf. Fig. 2). Here, we report on electrical transport measurements on a $GdRh_2Si_2$ single crystal, with current parallel and perpendicular to the crystallographic c-direction. The temperature dependence of the electrical resistivity, $\rho(T)$, for these two current directions is presented in Fig. 8. The absolute value for the in-plane resistivity $j \perp 001$ at room temperature was about 75 μΩ cm. Irregularities in the cross section of the sample made it impossible to estimate a reliable absolute value for current flow parallel to the [001]-direction, therefore we present for this direction only the relative values, $\rho/\rho_{300\ K}$. For both directions, the resistivity shows a linear-in-temperature behavior from $T=300$ K down to the AFM phase transition. At $T_N \approx 107$ K a change of the slope in the resistivity curves occurs. Below T_N, the decrease of the resistivity becomes stronger if the current flows perpendicular to the [001]-direction. For j parallel to the [001]-direction, the resistivity increases below T_N and drops down after reaching a maximum at about $T=90$ K. This can be understood as a change of the Fermi surface since the periodicity in the lattice becomes larger when entering the AFM phase. In result, more states near the Fermi level that contribute to the conductivity exist for current perpendicular to the [001]-direction and less for current parallel to the [001]-direction.

In comparison to previous work [21], where electrical transport measurements were performed on a polycrystalline sample of $GdRh_2Si_2$ with $\rho_{200\ K}/\rho_{1.8\ K} \approx 9$, the sample quality was improved with $RR_{1.8\ K} = \rho_{300\ K}/\rho_{1.8\ K} \approx 23$ ($\rho_{200\ K}/\rho_{1.8\ K} \approx 17$) determined for the $j \perp 001-$direction of the single crystals.

4. Summary

Single crystals of $GdRh_2Si_2$ were grown by a modified Bridgman method from indium flux. The optimization of the temperature profile during the growth led to mm-sized single crystals with a platelet habitus. The specific heat of $GdRh_2Si_2$ shows a sharp λ-type anomaly at $T=107$ K, establishing a second order phase transition into the AFM ordered phase. The data can be described by $C/T = \gamma_0 + \beta T^2$ with the Sommerfeld coefficient $\gamma_0 \approx 4$ mJ/mol K^2 for $T < 5$ K. The Debye temperature $\Theta_D \approx 148$ K was determined from the slope β of the linear fit. Magnetic measurements on the single crystals show the ordering of the Gd^{3+} moments at $T_N=107$ K and a spin flop transition at $B_{sf} \approx 1$ T with an external field applied along the [100]-direction of the tetragonal lattice. The effective magnetic moment $\mu_{eff} = (8.28 \pm 0.10)\mu_B$ agrees well with values from the literature, and is larger than the theoretically predicted value of $\mu_{eff} = 7.94\mu_B$. The determined Weiss temperature, $\Theta_W = (8 \pm 5)$ K, is much smaller than T_N, indicating a pronounced competition between antiferromagnetic and ferromagnetic interactions. Electrical transport data show a large anisotropy for current flow parallel and perpendicular to the [001]-direction below T_N. The residual resistivity ratio $RRR = \rho_{300\ K}/\rho_0 \sim 23$ shows that we succeeded in growing high-quality crystals from a high-temperature indium flux.

Acknowledgments

We thank C. Geibel, K. Kummer, and D.V. Vyalikh for valuable discussions and K.-D. Luther for technical support.

References

[1] S. Quezel, J. Rossat-Mignod, Solid State Commun. 49 (1984) 685–691.
[2] O. Trovarelli, C. Geibel, S. Mederle, C. Langhammer, F.M. Grosche, P. Gegenwart, M. Lang, G. Sparn, F. Steglich, Phys. Rev. Lett. 85 (2000) 626–629.
[3] S. Seiro, C. Geibel, J. Phys.: Condens. Matter 26 (2014) 046002.
[4] A. Chikina, M. Höppner, S. Seiro, K. Kummer, S. Danzenbächer, S. Patil, A. Generalov, M. Güttler, Yu. Kucherenko, E.V. Chulkov, Yu.M. Koroteev, M. Köpernik, C. Geibel, M. Shi, M. Radovic, C. Laubschat, D.V. Vyalikh, Nat. Commun. (2014), http://dx.doi.org/10.1038/ncomms4171.
[5] I. Felner, I. Nowik, Solid State Commun. 47 (1983) 831–834.
[6] I. Felner, I. Nowik, J. Phys. Chem. Solids 45 (1984) 419–426.
[7] G. Czjzek, V. Oestreich, H. Schmidt, K. Łatka, K. Tomala, J. Magn. Magn. Mater. 79 (1989) 42–56.
[8] M. Slaski, J. Leciejewicz, A. Szytuła, J. Magn. Magn. Mater. 39 (1983) 268–274.
[9] A. Szytuła, A. Budkowski, M. Slaski, R. Zach, Solid State Commun. 57 (1986) 813–815.
[10] E. Kwapulinska, K. Kaczmarska, A. Szytula, J. Magn. Magn. Mater. 73 (1988) 65–68.
[11] G.A. Cabrera-Pasca, A.W. Carbonari, R.N. Saxena, B. Bosch-Santos, J.A.H. Coaquira, J.A. Filho, J. Alloy Compd. 515 (2012) 44–48.
[12] P.C. Canfield, I.R. Fisher, J. Cryst. Growth 225 (2001) 155–161.
[13] P.C. Canfield, Z. Fisk, Philos. Mag. B 65 (1992) 1117–1123.
[14] C. Krellner, S. Taube, T. Westerkamp, Z. Hossain, C. Geibel, Philos. Mag. 92 (2012) 2508–2523.
[15] S. Wirth, S. Ernst, R. Cardoso-Gil, H. Borrmann, S. Seiro, C. Krellner, C. Geibel, S. Kirchner, U. Burkhardt, Y. Grin, F. Steglich, J. Phys.: Condens. Matter 24 (2012) 294203.
[16] J. Ferstl, New Yb-Based Systems: From an Intermediate-Valent to a Magnetically Ordered State, Cuvillier, Göttingen, 2007.
[17] K.H.J. Buschow, F.R. de Boer, Physics of Magnetism and Magnetic Materials, Kluwer Academic Publishers, New York, Boston, Dordrecht, London, Moscow, 2003.
[18] A. Nakamura, Y. Hiranaka, M. Hedo, T. Nakama, Y. Miura, H. Tsutsumi, A. Mori, K. Ishida, K. Mitamura, Y. Hirose, K. Sugijama, F. Honda, R. Settai, T. Takeuchi, M. Hagiwara, T.D. Matsuda, E. Yamamoto, Y. Haga, K. Matsubayashi, Y. Uwatoko, H. Harima, Y. Onuki, J. Phys. Soc. Jpn. 82 (2013) 104703.
[19] L.D. Tung, J.J.M. Franse, K.H.J. Buschow, P.E. Brommer, N.P. Thuy, J. Alloy Compd. 260 (1997) 35–43.
[20] A. Szytuła, J. Less-Common Met. 157 (1990) 167–171.
[21] G.A. Cabrera-Pasca, A.W. Carbonari, B. Bosch-Santos, J. Mestnik-Filho, R.N. Saxena, J. Phys.: Condens. Matter 24 (2012) 416002.